Reprinted from THE JOURNAL OF CHEMICAL PHYSICS, Vol. 26, No. 4, 815–823, April, 1957
Printed in U. S. A.

Dynamic Compression of Liquids from Measurements on Strong Shock Waves*

JOHN M. WALSH AND MELVIN H. RICE
Los Alamos Scientific Laboratory, Los Alamos, New Mexico
(Received July 2, 1956)

High explosives were used to drive strong shock waves into various liquids, and a moving-image camera was employed to determine velocities associated with the shock waves. The measured velocities are transformed to pressure-compression points by applying the conservation relations. The pressures attained vary among the 15 liquids studied but are typically in the range 50 kilobars to 150 kilobars. For water, more extensive experimentation suffices to determine the Hugoniot curve from 30 kilobars to 450 kilobars. The highest pressure for each of the liquids extends the available data range from static experimentation several fold.

A shock-wave-reflection experimental method is described, the purpose of which is to measure the useful thermodynamic variable $(\Delta H/\Delta V)_P$ at high pressures. Results are given for water.

Qualitative experiments to study the transparency of shocked water, carbon tetrachloride, ethyl alcohol, and benzene are reported.

INTRODUCTION

WHEN a mass element is traversed by a shock front, it suffers an almost discontinuous change in its thermodynamic state. The shock front propagates with a velocity, U_s, which is supersonic relative to the undisturbed medium; and a mass (or particle) velocity, U_p, is imparted to the material behind the shock front (see Fig. 1). The conservation relations[1] for the process are

$$P_1-P_0=U_sU_p/V_0, \qquad \text{Momentum} \qquad (1)$$

$$V_1/V_0=(U_s-U_p)/U_s, \qquad \text{Mass} \qquad (2)$$

$$E_1-E_0=\tfrac{1}{2}(P_1+P_0)(V_0-V_1), \qquad \text{Energy} \qquad (3)$$

where P_0, V_0, E_0 and P_1, V_1, E_1, denote pressure, specific volume and specific internal energy ahead of and behind the shock front respectively. Equation (3) may be written in terms of specific enthalpy, H,

$$H_1-H_0=\tfrac{1}{2}(P_1-P_0)(V_0+V_1), \qquad (3')$$

a form which will be useful in later considerations.

Since the specific internal energy for a material is some function of its pressure and specific volume, Eq. (3) may be regarded as an equation defining the locus in the P, V plane of all states attainable by propagating a shock wave into a given initial state P_0, V_0, E_0. This locus is defined as the Hugoniot curve centered at P_0, V_0.

Section I describes an experiment to determine a point on the Hugoniot curve of a liquid, the initial state (P_0,V_0) of the liquid corresponding to approximately standard conditions. Results are given for water, mercury, and thirteen organic liquids. The pressures attained vary with the liquid, maximum values ranging from 100 kilobars for ether and hexane to 450 kilobars for water and mercury (1 kilobar$=10^9$ dynes/cm^2 $=986.9$ atmos).

It is desirable to supplement the Hugoniot curves by the measurement of additional high-pressure states. A shock reflection experiment for obtaining such data is described in Sec. II, and results are given for water. The data serve to reduce the uncertainty in generalizing the Hugoniot curve into a more complete high-pressure equation of state for water. Such a calculation is the subject of the succeeding paper.

Section III is devoted to the description of a set of qualitative experiments to study the transparency of shocked liquids.

I. DETERMINATION OF HUGONIOT CURVES FOR LIQUIDS

A. Preliminary Remarks

A plane-wave high-explosive system is used to drive a shock wave into a 24ST aluminum plate. The shock wave propagates through the aluminum and into the liquid specimen, which is in contact with the front surface of the aluminum plate. 24ST aluminum is used because the equation of state of this material (for states attained in present experimentation) is accurately known from previous work. Use of the 24ST aluminum data permits the determination of the desired Hugoniot point from two easily measured velocities.

In the following, a photographic method to determine two appropriate velocities is described. The transformation of measured velocities to a pressure-compression point is then detailed. Data for the liquids are given, and error estimates are made.

B. Experimental Determination of Velocities

A typical shot assembly is illustrated as Figs. 2(a), 2(b), 2(c), and 2(d). Basic components of the system (except the details of the assembly on the front surface

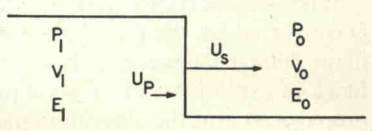

FIG. 1. Pressure-profile schematic drawing of a shock wave.

* Work done under the auspices of the U. S. Atomic Energy Commission.

[1] These three relations, called the Rankine-Hugoniot equations, are derived in any text on shock-wave hydrodynamics. See, for example, R. Courant and K. O. Friedrichs, *Supersonic Flow and Shock Waves* (Interscience Publishers, Inc., New York, 1948).

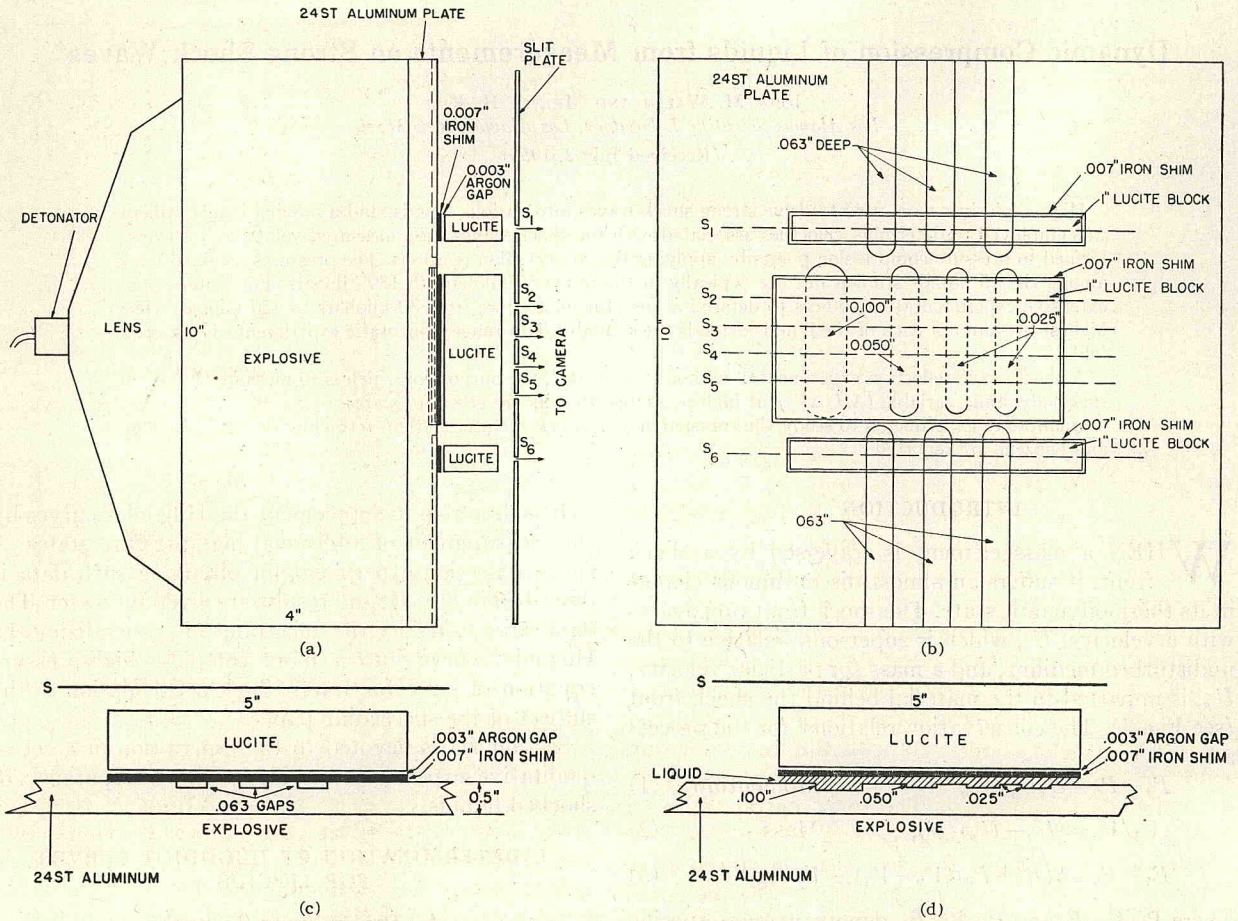

FIG. 2. (a) Side view of shot assembly. (b) Front view of Lucite-iron shim assembly. Viewing slit positions indicated by lines $S_1 \cdots S_6$. (c) Cutaway view of the assembly behind slit S_1 or S_6. Shim and gap thickness are exaggerated. (d) Cutaway view of the assembly behind slit S_2, S_3, S_4, or S_5.

of the 24ST aluminum plate) are easily identified by an inspection of Fig. 2(a). The moving image camera, not shown in the figure, views the assembly through six slits $S_1 \cdots S_6$ which are normal to the plane of the figure. The camera (in an underground bunker some ten feet from the assembly) is arranged to sweep the image in a direction normal to the slits.

The assembly on the front surface of the 24ST aluminum plate is illustrated as Figs. 2(b), 2(c), and 2(d). Ten flat-bottom grooves are milled into the surface of the plate. The six outer grooves [see Fig. 2(b)] are 0.063 in. deep. The four central grooves are [left to right in Fig. 2(b)] 0.100, 0.050, 0.025, and 0.025 in. deep. An iron shim and Lucite assembly is mounted over these grooves in the positions shown in Fig. 2(b). The cutaway view given as Fig. 2(c) details the assembly behind slit S_1 (or S_6). A similar view of the assembly behind S_2 (or S_3, S_4, S_5) is shown as Fig. 2(d).

When the shot is fired, point initiation at the detonator is converted by the plane-wave lens into an essentially plane detonation wave. This wave propagates across the block of explosive and causes a plane shock wave to be propagated into the aluminum plate. The interaction of this shock wave with the assembly on the front surface of the aluminum plate is as follows.

In the regions between and adjacent to the outer grooves [see Fig. 2(c)] the shock wave strikes the 0.007-in. iron shim, which then closes the 0.003-in. argon gap. At the groove positions, the shock wave strikes the groove bottom and causes it to traverse the 0.063-in. free-run distance with a velocity characteristic of that shock strength. When the aluminum free-surface strikes the iron shim over the groove, the 0.003-in. argon gap is closed violently. As the iron shim moves across the 0.003-in. argon gaps, it causes the argon, caught between the moving iron shim and the Lucite surface, to suffer multiple shock reflections and become brilliantly luminous.† It is this light which exposes the moving-image-camera-record. The photographic record from

† The illumination mechanisms are not precisely reproduced for positions between and above the grooves, since the iron shim shock strength is slightly different in the two cases. In either case aluminum and iron equation of state data, and graphical solution methods similar to those given in Sec. IC, suffice to determine the iron shim shock strengths. These shock strengths are essentially the same, and the small time difference in the indicated argon gap closure times is entirely negligible. Reproducibility of the illumination mechanisms is assumed in the record analysis.

these portions of the assembly is seen in Fig. 3, slits S_1 and S_6. The three portions of the trace caused by the groove bottoms are delayed in time (offset downward on the record). The magnitude of this time delay is determined by comparator readings of the record, combined with the known writing speed of the camera. This delay is the time required for the aluminum free-surface to traverse the groove depth, minus the time for the aluminum shock wave to traverse the same distance; i.e.,

$$\frac{1}{R_1}\equiv\frac{t_1}{d_1}=\frac{1}{U_{fs}}-\frac{1}{U_{sa}}, \tag{4}$$

where t_1 is the time offset measured from the record, d_1 is the depth of the groove, U_{fs} is the aluminum free-surface velocity and U_{sa} is the aluminum shock wave velocity. The six measurements of R_1 (which will be called the "reduced velocity") show a total scatter which is typically between 1% and 2% and the average has a probable error which is about 0.5%.

In the region of the central assembly [see Fig. 2(d)] the aluminum shock wave interacts with the aluminum-liquid interface and causes a shock wave to be transmitted into the liquid. The latter shock wave traverses the liquid specimen, interacts with the iron shim, and causes closure of the 0.003-in. argon flash-gap with accompanying luminosity. The four central traces of Fig. 3 are the moving-image-camera record from this portion of the assembly. It is seen that the traces lag at the groove positions, this lag indicating that the liquid shock wave is slower than the aluminum shock wave. The measured time delays, then, are related to the shock wave velocities by

$$\frac{1}{R_2}\equiv\frac{t_2}{d_2}=\frac{1}{U_s}-\frac{1}{U_{sa}}, \tag{5}$$

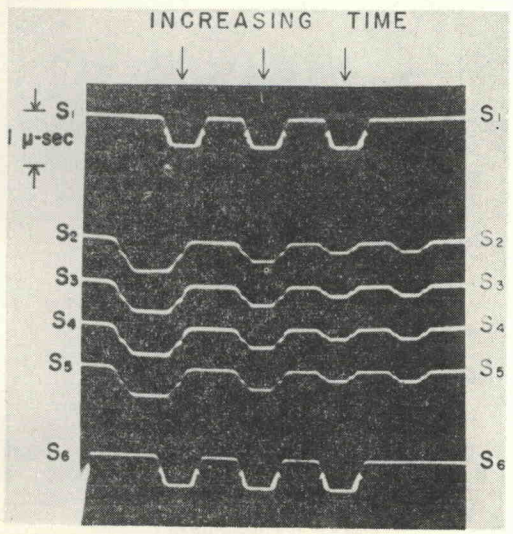

FIG. 3. A moving image camera photographic record from the assembly illustrated in Fig. 2.

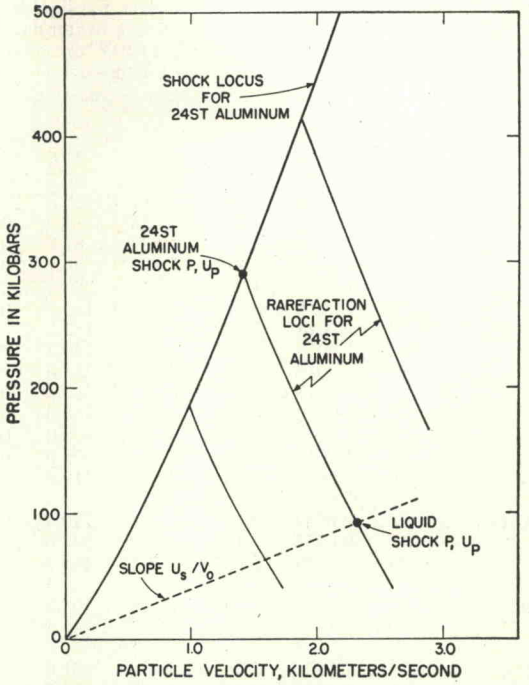

FIG. 4. Graphical solution to determine pressure and particle velocity for a liquid shock wave.

where t_2 is the time delay measured from the record, d_2 is the depth of the milled groove, U_s is the shock-wave velocity for the liquid, and U_{sa} is, as before, the shock-wave velocity for the aluminum. The purpose of the 0.025-in. liquid layer above the main aluminum plate is to insure that the 0.003-in. argon gap is closed at the same velocity at positions over the grooves and between grooves, so that consistent errors in measured time delays will be avoided. The purpose of the different groove depths is to insure that shock attenuation does not influence the measured reduced velocity, R_2. This precaution proved unnecessary, as the measured velocities for the various groove depths were the same within experimental error. The sixteen measurements of the reduced velocity show a percentage scatter which is quite different from shot to shot and depends upon the magnitude of $U_s^{-1}-U_{sa}^{-1}$; i.e., scatter for the reduced velocities is very large when U_s and U_{sa} are nearly equal. In all cases, however, the precision for U_s (obtained below from the measured reduced velocities and known U_{sa}) is good. The total scatter in U_s is typically 3% to 4%, and the average value of U_s has a probable error of about 0.5%.

C. Transformation of Measured Velocities to a Pressure-Compression Point

The average measured value of R_1 [Eq. (4)] is combined with the previously determined[2] experimental

[2] J. M. Walsh and R. H. Christian, Phys. Rev. **97**, 1544 (1955). Equation (6) is an analytical fit of 24ST aluminum data between $U_{fs}=1.6$ km/sec and $U_{fs}=6.5$ km/sec and is based on more extensive data than given in the preceding reference.

TABLE I. Experimental Hugoniot curve data for liquids. Velocities in km/sec, pressure in kilobars, V_0 in cc/g (water data, for which actual initial temperatures were 15°C to 30°C are corrected to the uniform initial state $T_0=20$°C, $P_0=1$ atmos).

Liquid	T_0 °C	V_0	U_s	U_p	P	V/V_0
Water	20	1.0018	3.354	0.952	31.8	0.716
	20	1.0018	4.093	1.392	56.8	0.660
	20	1.0018	4.126	1.411	58.2	0.658
	20	1.0018	4.536	1.655	74.9	0.635
	20	1.0018	4.813	1.829	87.8	0.620
	20	1.0018	4.777	1.806	86.1	0.622
	20	1.0018	4.757	1.798	85.4	0.622
	20	1.0018	5.626	2.385	133.9	0.576
	20	1.0018	5.604	2.370	132.5	0.577
	20	1.0018	5.601	2.335	130.5	0.583
	20	1.0018	8.07	4.13	333.0	0.488
	20	1.0018	8.07	4.24	342.0	0.475
	20	1.0018	8.45	4.60	388.0	0.456
	20	1.0018	8.49	4.72	400.0	0.444
	20	1.0018	8.59	4.72	405.0	0.450
	20	1.0018	8.74	4.81	419.0	0.450
Mercury	25	0.0739	2.752	0.608	226.4	0.779
	17	0.0739	3.101	0.772	324.0	0.751
	24	0.0739	3.504	0.978	463.7	0.721
Acetone	26	1.274	5.37	2.510	105.8	0.533
	30	1.279	3.97	1.495	46.4	0.623
Benzene	32	1.155	5.66	2.470	121.0	0.564
	16	1.133	4.10	1.448	52.4	0.647
Bromoethane	19	0.685	4.68	2.300	157.1	0.508
	16	0.682	3.40	1.363	68.0	0.599
Carbon Disulfide	33		4.32	2.412	129.5	0.441
	17		3.37	1.415	58.5	0.580
Carbon Tetrachloride	25	0.634	4.85	2.235	171.0	0.539
	22	0.629	3.51	1.325	73.9	0.622
Ethyl Ether	32	1.433	5.40	2.550	96.1	0.528
	21	1.407	3.88	1.517	41.8	0.609
Ethyl Alcohol	26	1.275	5.63	2.500	110.4	0.556
	21	1.267	4.03	1.487	47.3	0.631
Glycerine	30	0.798	6.07	2.240	170.3	0.631
	18	0.794	4.58	1.328	76.6	0.710
Hexane	32	1.499	5.54	2.590	95.7	0.533
	19	1.471	4.02	1.517	41.5	0.622
Methanol	24	1.271	5.51	2.525	109.5	0.542
	15	1.255	3.95	1.483	46.6	0.625
N-amyl Alcohol	23	1.236	5.81	2.465	115.9	0.576
	19	1.227	4.26	1.466	50.9	0.656
Toluene	4	1.138	5.73	2.412	121.5	0.579
	15	1.141	4.12	1.443	52.1	0.650
Mononitro-toluene	12	0.856	5.64	2.300	151.5	0.592
	12	0.856	4.20	1.340	65.8	0.681

curve for 24ST aluminum

$$U_{sa}=5.190+20.77\log_{10}\left(\frac{U_{fs}+10.895}{10.895}\right) \qquad (6)$$

(velocities in kilometers per second) to yield accurate values of aluminum shock velocity, U_{sa}, and aluminum free-surface velocity, U_{fs}. The value of U_{sa} thus obtained is combined with the average measured R_2 [Eq. (5)] to obtain the liquid shock velocity, U_s.

The velocities U_{sa} and U_s then suffice, when combined with known 24ST aluminum data and the usual hydrodynamic relations, to determine the desired pressure, particle velocity and compression for the shock wave in the liquid: The 24ST aluminum data necessary for this purpose are the pressure *versus* particle-velocity loci. The calculations used to determine these curves for aluminum are reviewed in Appendix I, and the curves are illustrated in Fig. 4. The curve that goes through the origin is the locus of all possible states attainable by propagating a right-going shock into normal 24ST aluminum which is initially at rest. Each cross curve, of which only three are illustrated, is then the locus of additional P, U_p states obtained when the shock wave is relieved by a left-going rarefaction wave.

The P, U_p state for the liquid shock wave can now be determined by graphical solution (see Fig. 4) from the boundary condition that P and U_p must be continuous across the aluminum-liquid interface: From Eq. (1), where $P_0=10^{-5}P_1$ and can be neglected, it is seen that the P, U_p state for the liquid must lie on a ray from the origin of slope U_s/V_0. The intersection of this ray with the appropriate aluminum rarefaction curve (i.e., the curve passing through the P, U_p point corresponding to the measured aluminum shock velocity) then satisfies the boundary conditions and hence gives the pressure and particle velocity for the state in the liquid shock wave. The corresponding specific volume and specific energy for the shocked liquid are then given by applications of Eqs. (2) and (3).

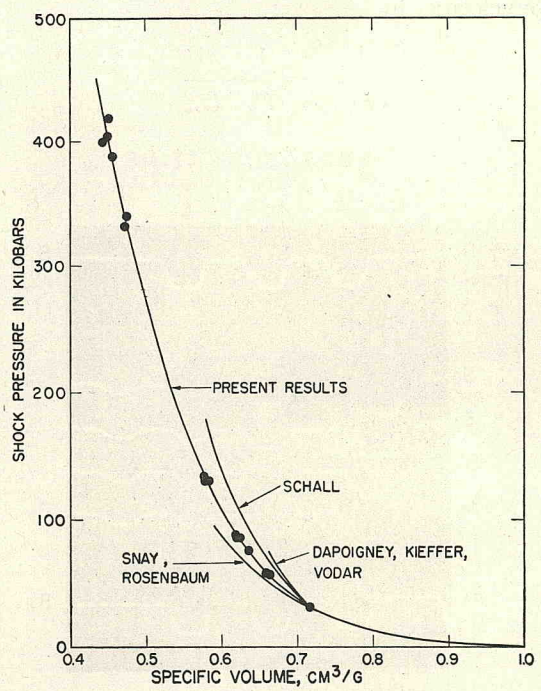

FIG. 5. Hugoniot curve for water.

Two slight modifications of the above procedures require special comment. First, in the mercury experiments a shock wave instead of a rarefaction wave is reflected into the 24ST aluminum from the aluminum-mercury interface. Hence the graphical solutions for mercury were carried out using the aluminum P, U_p curves corresponding to reflected shock waves (not shown in Fig. 4). Finally, some high pressure water experiments (330 kilobars to 420 kilobars) were performed by accelerating thin projectile plates with high explosive for distances from 1 to 3 in. The strong shock wave into the 24ST aluminum was caused by collision of the projectile plate with the back surface of the 24ST aluminum. Error per shot increased by about a factor of two, due to lack of planarity of the shock wave and an associated sacrifice in the number of identical measurements in each shot.

D. Experimental Hugoniot Curve Data

Experimental data for the fifteen liquids are listed as Table I. The Hugoniot curve for water, the most extensively investigated liquid, is plotted in Fig. 5. The present data may be compared to previous experimental contributions by Schall,[3] and by Dapoigny, Kieffer, and Vodar.[4]

Both efforts utilized an x-ray flash photographic method due to Schall. Their results, taken from graphs in the respective papers, are seen to indicate a considerably smaller compression for water than the present work. The offset between Schall's data and present data is about 5% in compression, $(V_0-V)/V_0$, at 80 kilobars and 8% at 180 kilobars.

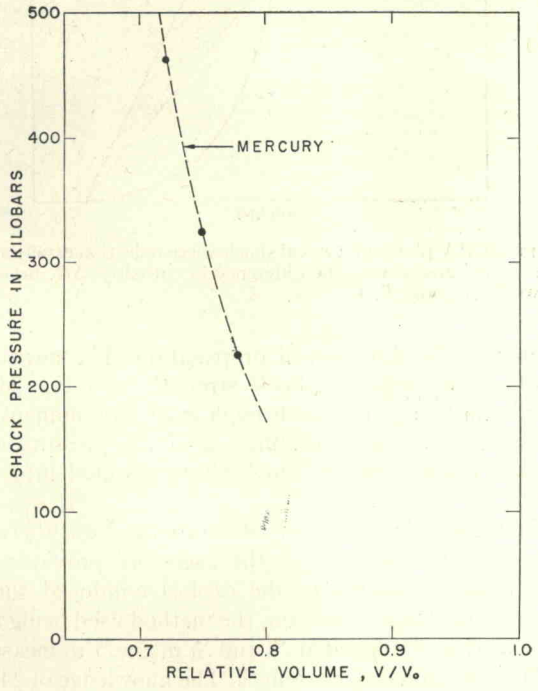

FIG. 6. Hugoniot curve for mercury.

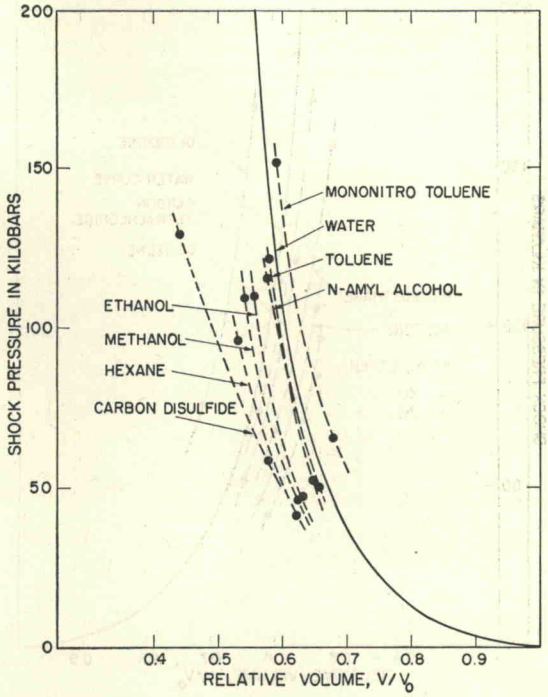

FIG. 7. Hugoniot curves for various organic liquids.

A number of theoretical-extrapolated approaches also have been employed to determine the Hugoniot curve for water, notably by Kirkwood and co-workers,[5–7] by Burkhardt,[8] and by Snay and Rosenbaum.[9] The latter effort, which incorporated the more complete experimental data then available, appears to be the most successful. Their resulting Hugoniot curve for water (based on Bridgman's isotherms to 35 kilobars,[10,11] high temperature data to 2.5 kilobars by Kennedy,[12] and extrapolation procedures) is seen in Fig. 5. The curve agrees with present results around 30 kilobars and deviates to the left at higher pressures, the compression offset at 95 kilobars being 5%.

[3] R. Schall, Z. angew. Phys. **2**, 252–254 (1950).
[4] Dapoigny, Kieffer, and Vodar, Acad. Sci. 215–217 (1954).

[5] J. G. Kirkwood and E. W. Montroll, "The pressure wave produced by an underwater explosion, II," Office of Scientific Research and Development (OSRD), No. 670 (June, 1942).
[6] J. G. Kirkwood and J. M. Richardson, "The pressure wave produced by an underwater explosion, III," Office of Scientific Research and Development (OSRD), No. 813 (August, 1942).
[7] Richardson, Arons, and Halverson, J. Chem. Phys. **15**, 785 (1947).
[8] W. Doering and H. Burkhardt, "Beitrage zur theorie der detonation," Air Materiel Command, Wright Field, Ohio, Air Documents Division.
[9] H. G. Snay and J. H. Rosenbaum, NAVORD Report 2383, "Shockwave parameters in fresh water for pressures up to 95 kilobars," U. S. Naval Ordnance Laboratory, White Oak, Maryland (April, 1952). These workers also employed Bridgman ice VII data to estimate possible (i.e., provided the freezing time is sufficiently short) effects of shock-induced freezing for water. Their results quoted above are for water which remains liquid; their freezing calculation is mentioned in Sec. III.
[10] P. W. Bridgman, J. Chem. Phys. **9**, 794 (1941).
[11] P. W. Bridgman, Proc. Am. Acad. Arts Sci. **74**, 399 (1942).
[12] G. C. Kennedy, Am. J. Sci. **248**, 540 (1950).

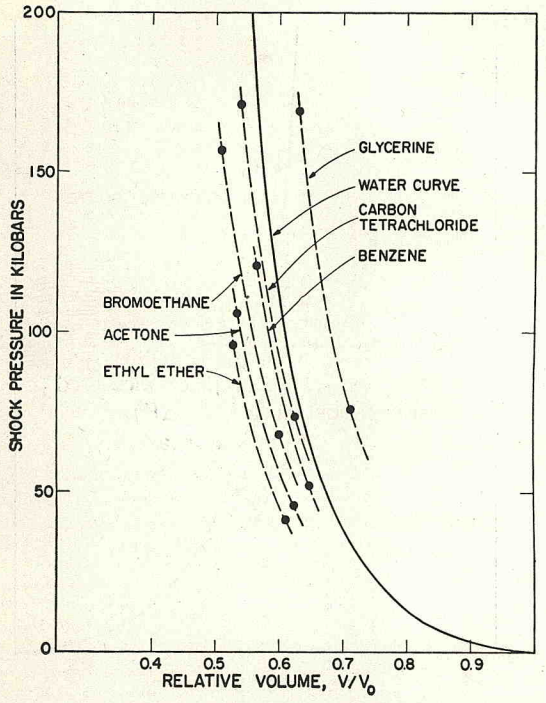

FIG. 8. Hugoniot curves for various organic liquids.

Hugoniot points for the remaining liquids are plotted as Figs. 6, 7, and 8. A number of indirect comparisons with present results are afforded by Bridgman's statically measured isotherms to 45 kilobars. A more direct comparison is made possible by converting the dynamic data to isotherms, or vice versa. In either case, small offsets due to thermal effects must be estimated. The comparison for water (succeeding paper) indicates excellent agreement between the static and dynamic results.

E. Error Estimates for Hugoniot Curve Data

Shot assembly and film reading uncertainties in the above experiments may be considered together as the sources of random error. The observed reproducibility of the water data indicates that the random probable error per data point is less than $\pm 1\%$ in compression for a given pressure. This result is also compatible with the error estimate one obtains from the observed scatter (see Sec. IB) within individual shots.

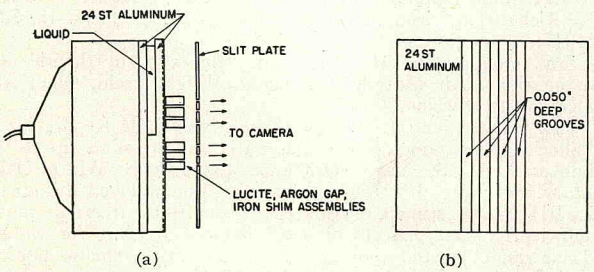

FIG. 9. (a) Side view of assembly for a shock-wave reflection experiment. (b) Front view of the 24ST aluminum plate showing positions of flat bottom grooves.

Two consistent errors in the above procedures are those associated with the use of 24ST aluminum as a standard, and the use of a previously measured camera writing speed in the determination of experimental velocities. The total uncertainty caused by use of aluminum data is discussed in Appendix I, where it is found to be $\pm 0.5\%$ or less (expressed as error in V/V_0 for a given pressure). Camera writing speed, determined to $\pm 0.1\%$ by separate experimentation, is sufficiently well known that it may be excluded as a source of significant consistent error.

II. SHOCK REFLECTION EXPERIMENTS FOR WATER

A water shock wave of known intensity is caused to interact with a 24ST aluminum-water interface which is normal to the direction of propagation. The measurement of the induced shock strength into the 24ST aluminum then permits (through mass and momentum conservations) the determination of the pressure and specific volume for the shock wave reflected into the water.

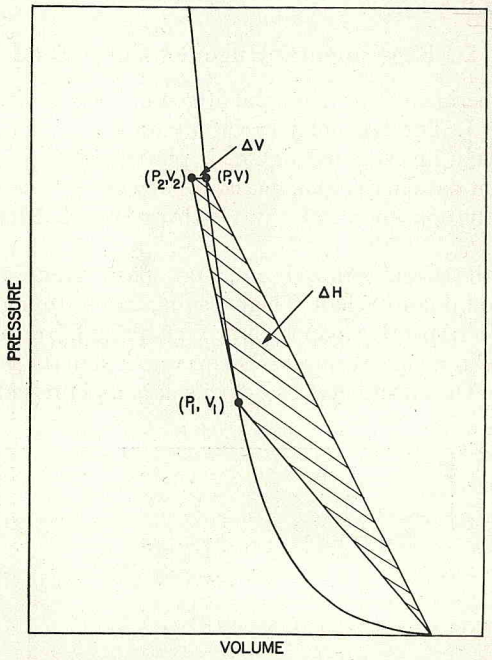

FIG. 10. P-V plot for a typical shock-wave reflection experiment. The shaded area equals the difference in enthalpy, ΔH, between points P_2, V_2, and P, V.

The experimental setup is illustrated as Figs. 9(a) and 9(b). The bottom half of the assembly provides for twelve measurements of the explosive-induced shock wave in the 24ST aluminum, the method used being the same as that employed at S_1 and S_6 in Sec. I to measure 24ST aluminum shock strength. The knowledge of 24ST aluminum shock strength permits the immediate determination of P_1, U_{p1} for the initial right-going shock into the water (given by the intersection of the 24ST

TABLE II. Data from water shock-reflection experiments.

	Initial shock					Reflected shock						
P_1 kbar	U_{p1} km/sec	V_1-V_0 cm³/g	E_1-E_0 kbar-cm³/g	H_1-H_0 kbar-cm³/g	P_2 kbar	U_{p2} km/sec	V_2-V_1 cm³/g	V_2 cm³/g	E_2-E_1 kbar-cm³/g	H_2-H_1 kbar-cm³/g	$\left(\frac{\Delta E}{\Delta P}\right)_v$ cm³/g	$\left(\frac{\Delta H}{\Delta V}\right)_p$ kbar
52.85	1.330	0.3347	8.8445	44.1007	106.7	0.620	0.0936	0.5735	7.46694	33.4032	0.4070	290.2
81.9	1.753	0.3752	15.3644	66.6830	160.8	0.881	0.0964	0.5302	11.9814	45.6358	0.4447	453.4
92.99	1.898	0.3874	18.0122	75.1452	182	0.977	0.0953	0.5191	13.1033	50.4464	0.4902	555.1
121.93	2.247	0.4141	25.2455	96.9039	235	1.206	0.0958	0.4919	17.0955	61.0352	0.5525	780.5

aluminum rarefaction locus and the experimentally determined P, U_p curve for water shock waves).

The top half of the assembly provides for twelve measurements of the shock wave transmitted into 24ST aluminum from the interaction at the front liquid-aluminum interface. The interface boundary conditions require that pressure and particle velocity for this aluminum shock are the same as those for the reflected shock wave into the water.

The applications of mass and momentum conservations [Eqs. (1) and (2)] to the above interactions give, for the water shock waves,

$$V_0-V_1=U_{p1}^2/(P_1-P_0)$$

and‡

$$V_2-V_1=(U_{p1}-U_{p2})^2/(P_2-P_1)$$

where P_1 and U_{P1} are the known pressure and particle velocity for the initial right-going shock into the water and P_2, U_{P2} are the known pressure and particle velocity for the reflected left-going shock. Specific internal energies, or specific enthalpies, are then given by application of Eq. (3) or Eq. (3′).

Data from shock reflection experiments are given as Table II. Results listed there incorporate small corrections for consistent errors arising from shock-wave degradation. The corrections, which are obtained from experimental 24ST aluminum degradation rates and equations of state for water and aluminum, are smaller in magnitude than estimated probable errors given below.

The enthalpy H_2 for the state (P_2,V_2) in the reflected shock wave may be compared with the enthalpy H for a state (P_2,V) on the Hugoniot curve centered at P_0, V_0. In particular, the ratio $(H-H_2)/(V-V_2)$, called $(\Delta H/\Delta V)_P$ below, is just the average value of the ratio C_P/α for the measured volume offset [i.e., $(\partial H/\partial V)_P \equiv C_P/\alpha$, where $C_P\equiv(\partial H/\partial T)_P$ and $\alpha\equiv(\partial V/\partial T)_P$]. See Fig. 10 for graphical interpretations of ΔH and ΔV.

The data $(\Delta H/\Delta V)_P$ *versus* pressure are plotted as Fig. 11. Over-all uncertainty in the curve, for the present data region 100 kilobars to 230 kilobars, is estimated at $\pm 15\%$ in $(\Delta H/\Delta V)_P$ for a given pressure. This large uncertainty, a consequence of taking differences between nearly equal experimental quantities, does not lead to large errors in the calculated P, V curves (succeeding paper) since $(\Delta H/\Delta V)_P$ is used only to evaluate small offsets from the measured Hugoniot curve.

‡ The state into which the reflected shock propagates is P_1, V_1, U_{p1} so that shock pressure is (P_2-P_1) and particle velocity due to the shock wave is $(U_{p1}-U_{p2})$. The laboratory system of coordinates is used for all velocities.

III. SHOCK-INDUCED FREEZING AND TRANSPARENCY OF SHOCKED LIQUIDS

Bridgman has reported pressure-induced freezing for nearly all liquids studied. Such freezing, as determined isothermally, is accompanied by a finite enthalpy release and volume reduction, all at constant pressure.

The P, V (Hugoniot) curve for shock waves, on the

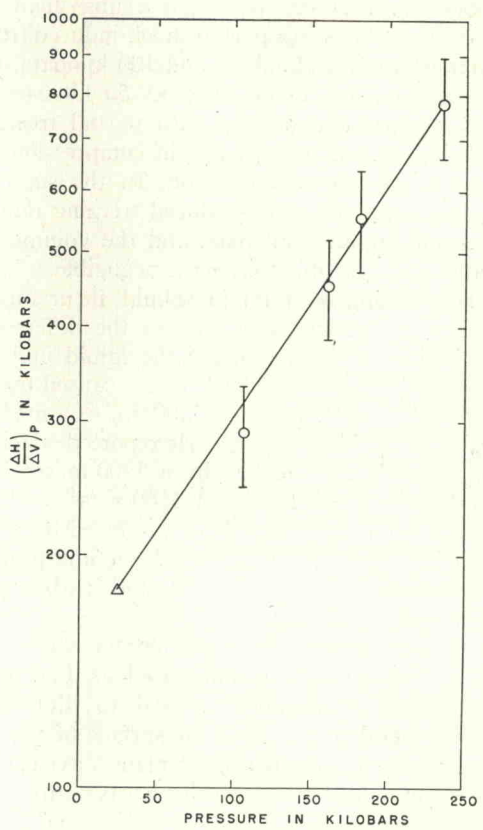

FIG. 11. Pressure *versus* $(\Delta H/\Delta V)_P$ for water. Data plotted as circles are taken from Table I. The point plotted as a triangle is based upon an interpretation of static data to 25 kilobars (see Appendix of succeeding paper).

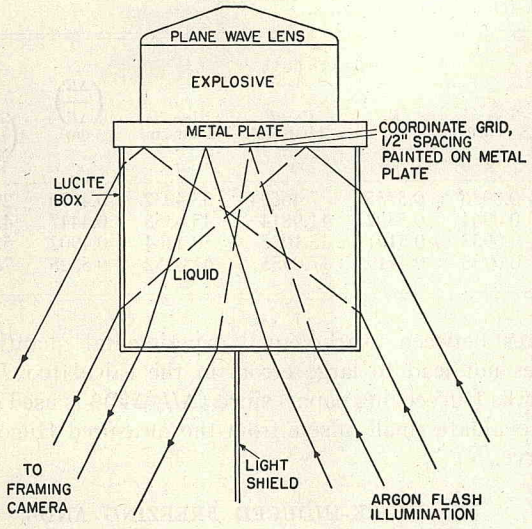

FIG. 12. Assembly for a transparency experiment.

other hand, is continuous, although the first derivative would suffer a discontinuity if freezing occurred. Doering and Burkhardt[8] estimated possible shock-induced freezing for water shock strengths above 27 kilobars and carbon tetrachloride shock strengths above 4 kilobars. Snay and Rosenbaum,[9] in a subsequent calculation, estimated possible partial shock-induced freezing for water between 27 kilobars and 100 kilobars, maximum freezing being about 20% at 50 kilobars. The volume decrement associated with partial freezing is small, being only about +2.5% in compression at 50 kilobars in the above calculation. In the succeeding paper, the estimated shock-induced freezing range for water is only about 5 kilobars, and the volume effect associated with possible freezing is negligible.

Partial freezing of a liquid should incur an associated loss of transparency, due to the difference in optical indices of refraction for the liquid and solid. H. Schardin[13] studied the shock waves caused by high-speed bullets (800 m/sec to 1800 m/sec) fired into carbon tetrachloride and water. He reported opacity for carbon tetrachloride shocked by a 1200-m/sec bullet, opacity for water shocked by an 1800-m/sec bullet and transparency for the water shock produced by an 800-m/sec bullet. These results have been interpreted as shock-induced freezing of water and carbon tetrachloride.

The present experimental method for the determination of transparency is illustrated as Fig. 12. An explosive-argon flash lamp is used to illuminate a 10×10 in. metal plate, the front surface of the latter being painted with coordinates. A plane-wave explosive system is employed to induce a shock wave into the back surface of the metal plate. This shock wave is transmitted through the metal plate and into the liquid specimen, which is in contact with the front (coordinated) surface of the metal. A framing (motion-picture-type) camera views the coordinates through the liquid shock wave. Successive pictures of the framing camera record are 1 μsec apart and the total time of observation is about 20 μsec. Photographic quality of the coordinates on the metal plate, as the shock wave propagates into the liquid, is a measure of the transparency of the shocked liquid.

Results of experimentation are given as Table III. The two pressures listed for each experiment cover the estimated range from the initial shock pressure in the liquid to the shock pressure corresponding to a time 20 μsec later. Water data, in particular, cover the pressure range 30 to 100 kilobars. No sign of opacity due to freezing was observed. Carbon tetrachloride, on the other hand, remains transparent for shock strengths below about 50 kilobars, although partial freezing for shock strengths in this pressure range would apparently be expected from thermodynamic arguments and the assumption of thermal equilibrium.[8] The observed opacity for strong carbon tetrachloride shock waves increases gradually with shock pressure, for pressures above about 70 kilobars.

It should be noted, in connection with the above results, that persistent (times of 1 sec order of magnitude and greater) super-cooled states are common to static high-pressure experimentation. In ordinary shock-wave experiments, on the other hand, any freezing must occur in a few microseconds (corresponding to shock propagation distances of a few inches), and it seems probable that the allotted time is usually inadequate. Even in the case of carbon tetrachloride (for which Bridgman notes rapid freezing) an association of observed high-pressure opacity and shock-induced freezing

TABLE III. Transparency of shocked liquids.

Liquid	Explosive (in inches)	Plate (in inches)	Shock pressures (kilobars)	Results
Water	4 (thick) baratol	1 (thick) Al	45–30	No apparent change as compared to the unshocked liquid
	4 comp *B*	1 brass	70–50	No change
	4 comp *B*	1 Al	100–70	No change
CCl_4	4 baratol	1 lucite, 1 brass, 1 lucite	15–10	No change
	4 baratol	1 brass	40–30	No change
	4 comp *B*	2 brass	50–35	No change
	Same	1 brass	80–60	Slight opacity[a]
	Same	½ brass	110–75	Pronounced opacity
	Same	½ Al	170–130	Complete opacity[b]
Benzene	4 comp *B*	1 Al	110–80	No change
Ethyl Alcohol	4 comp *B*	1 Al	100–70	No change

[a] The first picture after shock arrival exhibits a definite but slight reduction in coordinate definition. Coordinate definition suffers for about 3 μsec, then gradually improves (presumably due to decrease in shock intensity) until about 10 μsec after initial shock arrival. A further loss of coordinate definition (for two or three μsec) occurs at 10 μsec and is attributable to the arrival of a second shock wave (weak) at the brass-CCl_4 interface. The coordinates are visible in every picture and the last one (at 20 μsec) exhibits better definition than any other.

[b] Coordinates not visible in first picture after shock arrival and in all succeeding pictures. The CCl_4 shock front exhibits excellent reflectivity for the light from the argon flash.

[13] H. Schardin, "Problem der detonation," Schriften der Deuts Akad. Luft. (1941).

would seem dubious, since the observed shock-pressure threshold for opacity is an order of magnitude greater than the estimated value[8] for possible incipient freezing.

ACKNOWLEDGMENTS

The present work was made possible through the cooperation of a large number of people in the GMX Division of Los Alamos Scientific Laboratory.

We are especially grateful to Robert G. McQueen whose unpublished contributions to the equation of state of 24ST aluminum were used here, and to Robert G. Shreffler and Russell E. Duff for suggestions at various stages of this effort.

APPENDIX. PRESSURE *VERSUS* PARTICLE VELOCITY CURVES FOR 24ST ALUMINUM

The approximate relation

$$U_P \cong U_{fs}/2, \tag{A1}$$

the assumption of which is subsequently avoided by iteration, permits the immediate calculation of a Hugoniot curve for 24ST aluminum. The procedure is apparent from inspection of Eq. (A1), (6), (1) and (2).

The above Hugoniot curve, combined with the assumption

$$b \equiv (\partial P/\partial T)_v/C_v = \text{constant}, \tag{A2}$$

where b is evaluated from atmospheric pressure handbook data, permits the calculation of all adiabats which intersect the Hugoniot. The equation used to calculate adiabats is

$$\frac{dP_A}{dV}+bP_A=\frac{dP_H}{dV}-b\frac{d}{dV}\left[\frac{P_H}{2}(V_0-V)\right], \tag{A3}$$

where P_A and P_H are pressures on the adiabat and Hugoniot. This equation is obtained by differentiating $b \equiv (\partial P/\partial E)_v = (P_A-P_H)/(E_A-E_H)$ with respect to volume at constant entropy, and substituting Eq. (3) and $dE_A/dV = -P_A$.

The above-determined pressure-volume curves then permit the construction of the pressure, particle velocity curves through the relations

$$U_p=(P_H-P_0)^{\frac{1}{2}}(V_0-V_H)^{\frac{1}{2}}, \tag{A4}$$

$$U_r=\int_P^{P_H}\left(-\frac{dV}{dP_A}\right)^{\frac{1}{2}}dP_A \tag{A5}$$

The first expression, the particle velocity due to a shock wave, is a consequence of Eqs. (1) and (2). The second equation is just the Riemann integral for the particle velocity due to a simple rarefaction wave centered at a point P_H, V_V on the Hugoniot curve.

Finally, the approximation (A1) is removed by iteration. To do this, an improved value of U_p/U_{fs} is calculated from

$$U_p/U_{fs}=U_p\Big/\left[U_p+\int_0^{P_H}\left(-\frac{dV}{dP_A}\right)^{\frac{1}{2}}dP_A\right]$$

since the free-surface velocity is just the sum of the shock particle velocity and the Riemann integral to $P=0$. This ratio, which varies with shock strength, forms the basis for a refinement of Eq. (A1), the refined ratio then being used to determine a new set of curves. The calculation is iterated until the input ratios U_p/U_{fs} regenerate themselves to the desired accuracy, a process which was found to be rapidly convergent.

There are two errors in the above results for aluminum, both of which affect the liquids data.

First, the probable error in the aluminum experimental curve, Eq. (6), is approximately $\pm 0.3\%$ in shock velocity for a given free-surface velocity. A change of $\pm 0.3\%$ in the aluminum shock velocity curve (when traced through the analysis procedure given in Sec. IC) causes a change in liquids data which is also about $\pm 0.3\%$ in compression, $\Delta V/V_0$, for a given pressure.

The second uncertainty in aluminum results is caused by the approximation that $b \equiv (\partial P/\partial E)_v$ is a constant, Eq. (A2). This approximation, however, enters the calculation only as an estimate of the small offsets between calculated P, V curves (aluminum Hugoniot and adiabats), and it is easy to demonstrate that present liquids results are extremely insensitive to error in the assumed value of b. For example, if b were changed§ by 100% it would cause the P, U_p curves of Fig. 4 to shift by an amount everywhere less than 1% of U_p. Use of the perturbed aluminum curves, to perform the graphical solutions described in Sec. IC, causes a slightly smaller percentage change in the final liquids data, expressed as error in compression for given pressure. Hence, any reasonable error in the approximation apparently leads to negligible error in the liquids data.

§ This implies a zero thermal expansion for aluminum, if b were made zero. It can also be shown to lead to $(\partial^2 V/\partial P^2)_s < 0$ for high pressure, low entropy states if b were arbitrarily doubled. More extensive calculations for aluminum will be given in a future publication dealing with solids.